Simulation of non-Abelian gauge theories with optical lattices

L. Tagliacozzo,[1,*] A. Celi,[1,†] P. Orland,[2] and M. Lewenstein[1,3]

[1] *ICFO - The Institute of Photonic Sciences, Av. C.F. Gauss 3, E-08860 Castelldefels (Barcelona), Spain*
[2] *Baruch College and the Graduate School and University Center, CUNY, New York, NY 10010, USA*
[3] *ICREA-Institució Catalana de Recerca i Estudis Avancats, 08010 Barcelona, Spain*

Many phenomena occurring in strongly correlated quantum systems still await conclusive explanations. The absence of isolated free quarks in nature is an example. It is attributed to *quark confinement*, whose origin is not yet understood. The phase diagram for nuclear matter at general temperatures and densities, studied in heavy-ion collisions, is largely conjectural. Finally, we have no definitive theory of high-temperature superconductivity. Though we have theories that could underlie such physics, we lack the tools to determine the experimental consequences of these theories. *Quantum simulators* may provide such tools. Here we show how to engineer quantum simulators of non-Abelian lattice gauge theories. The systems we consider have several applications: they can be used to mimic quark confinement or to study dimer and valence-bond states (which may be relevant for high-temperature superconductors).

Gauge theories (GT) [1] provide the basis of modern physics. In the "Standard Model of Particle Physics" [2] GT describe three of the four fundamental interactions (namely "electromagnetic", "weak", and "strong" interactions. The last is described by the GT known as Quantum Chromo-Dynamics (QCD) [3]). Gauge symmetry plays also a role in General Relativity. At the same time, GT are present in many effective models of condensed matter, *e.g.* antiferromagnets [4] and high-temperature superconductors [5, 6]. Recently, the study of phase diagrams of various GT has gained new attention, because of the discovery of topological order. Due to their stability against perturbations, topologically-ordered phases may lead to feasible quantum computers [7–11].

Despite the enormous importance of GT, they defy solution. Wilson's formulation [12] of lattice gauge theories (LGT), where continuous space-time is replaced by a discrete set of points, provided the first computational tool to study the strong coupling regime. Monte-Carlo (MC) simulations of LGT is the main tool to compare strongly-coupled aspects of QCD with experiments [13]. What is hard or impossible to compute with MC remains out of reach. For example, the mechanism of charge confinement [14], invented to explain the absence of isolated quarks [15], is still debated four decades since first proposed. Furthermore, MC simulations cannot yet provide definite predictions for hot and dense nuclear matter [16, 17], probed by heavy nuclei collisions at CERN and RHIC [18, 19]. GT are also invoked in explanations of spin-liquid phases of antiferromagnets [4] and high-temperature superconductivity [20].

Recent progress in the experimental control of quantum systems makes possible to engineer systems that perfectly mimic theoretical models. This is the idea of *quantum simulators* [21–26], whose ultimate goal is to simulate GT, e.g. QCD, providing experimental access to their phase diagrams at finite temperature and density. A more modest goal is to emulate QCD, *i.e.* to find a model sharing its interesting properties, whose realization may be simpler than the full theory. The first steps of this emulation program were to describe quantum simulations of Abelian LGT [27–31]. The presence of many-body interactions, beyond nearest neighbors, has been the main technical obstacle. This obstacle has been addressed in [28], by using mesoscopic Rydberg gates [32].

Here we show how to simulate, using Rydberg atoms [33, 34], *non-Abelian gauge magnets* or *link models*, introduced in [35–37]. The models have two regimes, namely the strong- and weak-coupling regime. We discuss here the origin of charge confinement in both regimes, stressing the different physical origin in each. We propose how to identify the flux-tubes connecting static external charges in each of these regimes, and provide the experimental protocol to observe these flux tubes. We conclude by discussing a qualitative technique, based on energy landscapes around static charges, to identify in a generic LGT whether chromo-electric strings, *i.e.* charge confinement, is present.

THE MODEL

The quantum degrees of freedom of SU(2) gauge magnets are four states assigned to each link of the lattice. To have a GT, we need two sets of operators, $S = \{\,\Xi, \tilde{\Xi}\,\}$ and $D = \{\,\Gamma^a\,\}$, for $a = 0, \ldots, 4$ defined by

$$\Xi(\vec{\alpha}) = |0\rangle\langle 0| \otimes \exp(i\vec{\alpha}\cdot\vec{\sigma}) + |1\rangle\langle 1| \otimes I, \qquad (1)$$

$$\tilde{\Xi}(\vec{\alpha}) = |0\rangle\langle 0| \otimes I + |1\rangle\langle 1| \otimes \exp(i\vec{\alpha}\cdot\sigma), \qquad (2)$$

where $\vec{\alpha} = (\alpha_1, \alpha_2, \alpha_3)$ is real three-component vector and $\vec{\sigma} = (\sigma_1, \sigma_2, \sigma_3)$ are the Pauli matrices, and

$$\Gamma^0 = \sigma_1 \otimes I,\ \Gamma^j = \sigma_2 \otimes \sigma^j,\ j = 1, 2, 3,\ \Gamma^5 = \sigma_3 \otimes I. \quad (3)$$

The operators in the set S produce gauge transformations. Specifically in the absence of external charges, we

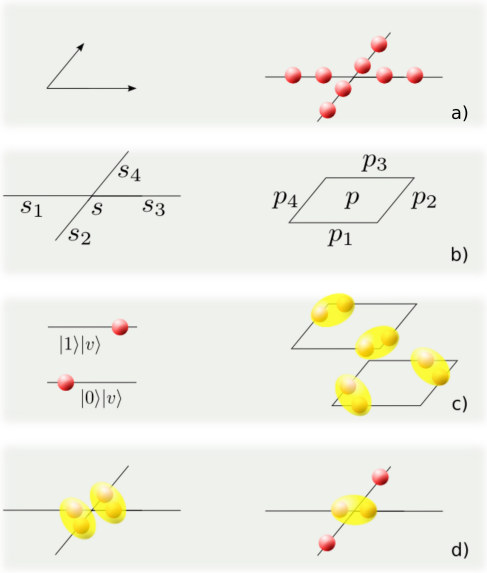

Figure 1. *The basics of non-Abelian gauge magnets* a) We assign to each link of an oriented lattice (left), the Hilbert space of two qubits, each of them represented by a sphere (right). b) A link may be labeled in either of two equivalent ways: by adding a subscript referring to the adjacent site (left panel), or to the adjacent plaquette (right panel). We number these labels counterclockwise. In both cases, links possess the original orientation of the lattice. c) On each link, one of the two qubits, the "position" qubit, determines the location of the other, the "spin" qubit, on the link. In this way, a red sphere on the left of a link represents the state $|0\rangle|v\rangle$, while a red sphere on the right of a link represents the state $|1\rangle|v\rangle$. Here $|0\rangle$ and $|1\rangle$ are eigenvectors of σ_3, with eigenvalues -1 and 1, respectively. Gauge invariance forces qubits adjacent to a site to form singlets (represented by yellow ovals around these sites). For an isolated plaquette (right panel), the gauge-invariant Hilbert space is two dimensional. The two configurations of singlets are orthogonal, because they differ by the value of their position qubits. d) For a generic lattice, the gauge condition acts on the "crosses" of links adjacent to a given site. This condition forces the qubits adjacent to that site into a singlet configuration. In the left panel, we show one of the two linearly-independent configurations with four qubits adjacent to the site making a singlet. On the right, we show a configuration with only two adjacent qubits to the site forming a singlet.

define a set of local symmetry operators

$$G_s(\vec{\alpha}) = \tilde{\Xi}(\vec{\alpha})_{s_1} \otimes \tilde{\Xi}(\vec{\alpha})_{s_2} \otimes \Xi(\vec{\alpha})_{s_3} \otimes \Xi(\vec{\alpha})_{s_4}, \quad (4)$$

on the "crosses", which consist of the four spin states adjacent to given site s (labeled $s_1, \ldots, s_4$. See Fig. 1 b)). The gauge-invariance constraint selects physical states

$$\{\ |\psi\rangle\ \} : G_s(\vec{\alpha})\,|\psi\rangle = |\psi\rangle\,, \forall s, \vec{\alpha}. \quad (5)$$

It is sufficient to impose this condition for $\vec{\alpha}$ equal to $\hat{x} = (1,0,0)$, $\hat{y} = (0,1,0)$, and $\hat{z} = (0,0,1)$.

The Hamiltonian H must commute with all the symmetry constraints (4). As explained in detail in [36], H is obtained by introducing parallel-transport operators on each link. The space of operators D is extended to include operators U, which act the auxiliary spin-1/2 space V. Explicitly

$$U = \Gamma^0 \otimes 1 - i \sum_{j=1}^{3} \Gamma^j \otimes \tau^j, \quad (6)$$

Here τ^j, $j = 1,2,3$ is a Pauli matrix on V. The commutation relations of the operators U and Ξ, $\tilde{\Xi}$ are

$$[\Xi(\vec{\alpha}), U] = \exp(i\vec{\alpha}\cdot\vec{\tau})U,\ [U, \tilde{\Xi}(\vec{\alpha})] = U\exp(-i\vec{\alpha}\cdot\vec{\tau}), \quad (7)$$

as expected for a consistent non-Abelian GT. We now have enough machinery to write the Hamiltonian:

$$\frac{H}{\Delta} = \sum_l \Gamma_l^5 + \frac{1}{g}\sum_p \mathrm{tr}(U_{p_1}\otimes U_{p_2}\otimes {U_{p_3}}^\dagger \otimes {U_{p_4}}^\dagger) + H.c., \quad (8)$$

where Δ is an energy scale, l denotes the links of the lattice, and p denotes the elementary plaquettes of the lattice ($p_1, \ldots, p_4$ being the links around the plaquette p, ordered as in Fig. 1 b)). The trace refers to the V-space. The coupling constant g determines if the system is in the *weak-* or in the *strong-coupling* regime ($g \to 0$ and $g \to \infty$, respectively).

In the presence of a static charge at the site $\tilde{s}$, the symmetry constraint at that site is modified to

$$G_{\tilde{s}}(\vec{\alpha})\,|\psi\rangle = \exp\left(i\vec{\alpha}\cdot\vec{S}\right)|\psi\rangle\,, \forall\vec{\alpha}, \quad (9)$$

where $\vec{S}$ is the spin-representation of possible charges, $1/2, 1, 3/2, 2$. Here we focus on the case of spin-1/2 charges, *i.e.* $\vec{S} \equiv \vec{\sigma}$. In this case the charge is encoded by a qubit located at $\tilde{s}$ and (9) can be expressed as

$$G^{ext}_{\tilde{s}}(\vec{\alpha})\,|\psi\rangle = |\psi\rangle\,, \forall\vec{\alpha} \quad (10)$$

with $G^{ext}_{\tilde{s}}(\vec{\alpha}) = G_{\tilde{s}}(\vec{\alpha}) \otimes \exp\left(i\vec{\alpha}\cdot\vec{\sigma}_{\tilde{s}}\right)$.

THE CONFINEMENT PHASE

The form of operators S and D suggests writing the Hilbert space of one link as $\mathcal{P}\otimes\mathcal{S}$, which is isomorphic to $\mathcal{C}^2 \otimes \mathcal{C}^2$. We interpret this decomposition as describing qubits (the right factor, $\mathcal{S}$) moving between the two ends of the links (the left factor, $\mathcal{P}$). In accord with equations (1), (2), and (3), we identify the basis of $\mathcal{P}$, $|0\rangle$ and $|1\rangle$, with the left-end (lower-end) or the right-end (upper-end) of a link in the x (y) direction. In this way, we represent the qubit $|0\rangle|v\rangle$ ($|1\rangle|v\rangle$) as a solid dot on the left (right) part of the link, cf. Fig 1 c). The operator $\Xi(\vec{\alpha})$ acts on those vectors in the left (down) two-dimensional subspace $|0\rangle|v\rangle$ of the x (y) oriented link (rotating them by $\exp\left(i\vec{\alpha}\cdot\vec{\sigma}\right)$). The operator $\tilde{\Xi}(\vec{\alpha})$ acts similarly on the other subspace of that link. Hence, the physical-state

condition (5) forces the total spin of the qubits adjacent to the site s to be zero, *i.e.* the creation of singlet among pairs of those, $S_{ij} \equiv \frac{1}{\sqrt{2}}(\uparrow\downarrow - \downarrow\uparrow)$, cf. Fig. 1 d).

At *weak-coupling*, H in (8) reduces to its plaquette terms. In analogy with the Abelian case [28], we exploit the bi-partite nature of the lattice. We imagine coloring the plaquettes red and black in a checker-board pattern. Next we consider the Hamiltonian (8), but including only half the terms, *e.g.* those on the black plaquettes. With this choice, the model becomes exactly solvable. As illustrated in Fig. 2 a), the ground state $|\Omega\rangle_0$ is a product state of single plaquette configurations,

$$|\Omega\rangle_0 = \prod_p |\phi\rangle_p \,, \text{ with } |\phi_p\rangle = \frac{1}{\sqrt{2}} \left(|\lambda_p\rangle + |\rho_p\rangle\right), \quad (11)$$

where $|\rho_p\rangle = |1\rangle_{p_1} |0\rangle_{p_2} |0\rangle_{p_3} |1\rangle_{p_4} S_{p_1,p_2} S_{p_3,p_4}$, and $|\lambda_p\rangle = |0\rangle_{p_1} |1\rangle_{p_2} |1\rangle_{p_3} |0\rangle_{p_4} S_{p_1,p_4} S_{p_2,p_3}$. We separate the "position" part of the Hilbert space from its "spin" part by writing the states as elements of $\mathcal{P}^{\otimes 4} \otimes \mathcal{S}^{\otimes 4}$. Both $|\rho\rangle$ and $|\lambda\rangle$ are represented in Fig. 1 c). The state $|\Omega\rangle_0$ factorizes into resonating-dimer states. Furthermore, each link, as a consequence of gauge invariance, is entangled with the rest of the system.

We now turn to confinement. Adding a pair of spatially separated external charges rearranges the singlets into strings connecting the charges. Each string causes long-range entanglement (LRE) between the charges, a distinctive feature of non-Abelian LGT. In an Abelian LGT, indeed, a single string does not induce entanglement, since typically it involves flipping a line of spins [38]. There, the unique source of LRE between charges is caused by the linear superposition of several orthogonal string states, present also here.

The ground state is indeed a superposition of string states along paths determined by both gauge invariance and energy minimization. A string passing through a plaquette increases its energy by $\delta E \propto \Delta/g$. Hence, strings touch as few plaquettes as possible. The number of excited plaquettes is proportional to the inter-charge distance, *i.e.* the charges are confined with a string tension proportional to Δ/g . This phenomenon is equivalent to the chromo-electric flux-tube expected in QCD between two colored charges. The simplest system exhibiting such behavior consists of only two plaquettes (Fig. 2 b).

At *strong-coupling*, the plaquette term in (8) may be neglected. The ground state is the configuration with all the position qubits in the state $|0\rangle$. Hence at any site s the spin qubits on s_3, s_4 form a singlet, see Fig 2 c) left. This is a product state of entangled "half-plaquettes", of the form $\prod_s |0\rangle_{s_3} |0\rangle_{s_4} S_{s_3,s_4}$.

If we now insert two static charges, a line of singlets must readjust. As consequence of (10), the two spin qubits $Q_{\tilde{s}_3}$, $Q_{\tilde{s}_4}$, originally forming the singlet at $\tilde{s}$, rearrange. One qubit, say $Q_{\tilde{s}_4}$ forms a singlet with the external charge, while the position state associated to the other qubit $Q_{\tilde{s}_3}$ changes from $|0\rangle$ to $|1\rangle$, i.e. the qubit moves to the opposite end of the link. There, by (5), it is forced to form a singlet with one of the two qubits of the same cross. The process repeats until one of the displaced qubits reaches the the second external charge. The result is a gauge-invariant string, stretching between the charges. The string is a line of qubits in state $|1\rangle$. The energy of each of them increases by 2Δ; therefore,

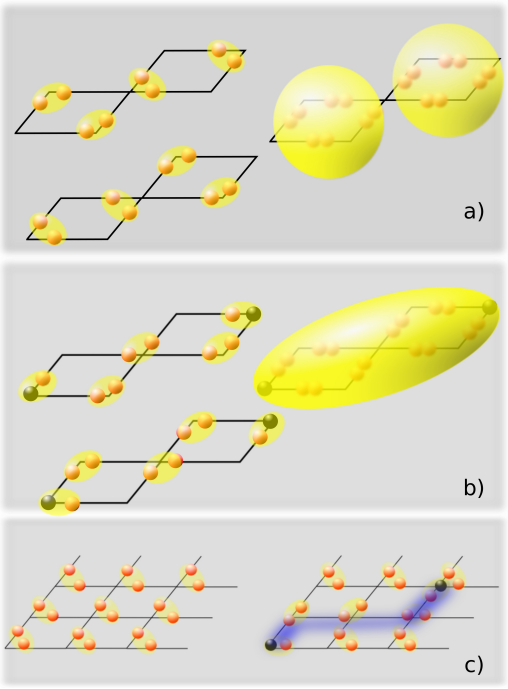

Figure 2. *Confinement of charges.* a), b) **Weak coupling**. a) In absence of external charges, dimers resonate on configurations allowed by gauge invariance. We show two such dimer configurations on the left side. The lowest-energy eigenstate is a product state of plaquette made of resonating dimers, depicted as yellow spheres. b) When two static charges are inserted, plaquettes are entangled by strings of singlets. These strings resonate among gauge-invariant minimal-energy configurations (cf. left panel). In this way, a "macromolecule" or "polymer", as large as the separation of the charges, is formed. We show the polymer in the right panel as a yellow oval. The energy of such a state rises linearly with the inter-charge separation, thereby confining charges. c) **Strong-coupling**. The ground state of (8) is the ordered configuration where all position qubits are in the state $|0\rangle$ and the spin qubits are forced by (5) to form singlets. This can be visualized by covering the lattice with singlets each formed by the two qubits positioned left-down on the x-y links exiting a site (left panel). When two external charges are inserted (black spheres), the singlets have to rearrange in order to respect the gauge constraint (10) (right panel). Some of the position qubits are flipped to $|1\rangle$ with an associated energy cost. Pictorially the corresponding spin qubits shift right-up on the x-y links. A string can be identified by position qubits in state $|1\rangle$, that is those spin qubits placed on the right-up of x-y links (a shaded blue line). The energy cost of a string is proportional to its length, hence, the charges are confined.

the static charges are confined. Note that the the actual ground state is a superposition of orthogonal strings states inducing LRE between the external charges. However, each single string already entangles the two charges, footprint of a non-Abelian LGT.

REALIZATION THROUGH RYDBERG ATOMS

To properly define the physical-state condition (4) and the plaquette terms in the Hamiltonian (8), we require eight-qubit interactions on neighboring sites. We can obtain long-range dipole interactions in an optical lattice by exciting atoms to Rydberg states. With single-site addressing, the Rydberg dipole can be switched on and off at will. This property is basic to the mesoscopic Rydberg gate of [32, 33]. This gate can conditionally transfer the population between two atomic levels of a multi-atomic system at once, depending on the state of a "control" atom. Here we exploit this gate to engineer both a digital and a mixed digital-analog quantum simulator of the Hamiltonian (8).

The qubits are atoms with two (meta)stable ground states trapped on the links of an holographically designed optical lattice [39], Fig 3 a). Each link contains two atoms (red spheres representing both the position and the spin qubits). Additional two-level atoms are placed at the sites and at the center of the plaquettes of the lattice (blue spheres in Fig. 3 a)) to control the Rydberg gates. Geometrically, eight ensemble atoms, belonging to the four links around a plaquette or entering a site, are positioned inside the Rydberg blockade of the controls (shaded cyan and orange regions in Fig. 3 a)). All the atoms are in a Mott state, and are thereby fixed in position.

The experiment we propose (similar to the one in [28]) requires three phases: one can first prepare the ground state of the system for any g, both in i) absence and in ii) presence of static external charges and finally iii) observe the confinement of external charges by unveiling the chromo-electric strings joining them and measuring their tension.

At *weak-coupling*, for the model with half of the plaquettes on, i) is achieved by adiabatic evolution. The starting configuration can be chosen, *e.g.* as the product state $\prod_{l_h}(|+\rangle \otimes |1\rangle)\prod_{l_v}(|+\rangle \otimes |0\rangle)$, where l_h and l_v are the horizontal and the vertical links of the lattice, respectively, and $|+\rangle \equiv \frac{1}{\sqrt{2}}(|0\rangle + |1\rangle)$, so that it has non-zero overlap with $|\Omega_0\rangle$ of (11). The evolution is performed for a time T ($\propto g/\Delta$) using the Hamiltonian $H(t) = (1-\lambda(t))H_a + \lambda(t)(H + H_G)$, with the smooth function $\lambda(t)$ that fulfills $\lambda(0) = 0, \lambda(T) = 1$, and H_a is a gapped Hamiltonian having as a unique ground state the starting configuration. The presence of $H_G = -\tilde{\Delta}\sum_{s,\vec{\alpha}=\hat{x},\hat{y},\hat{z}}(G_s(\vec{\alpha}) + G_s(\vec{\alpha})^\dagger)$ enforces gauge

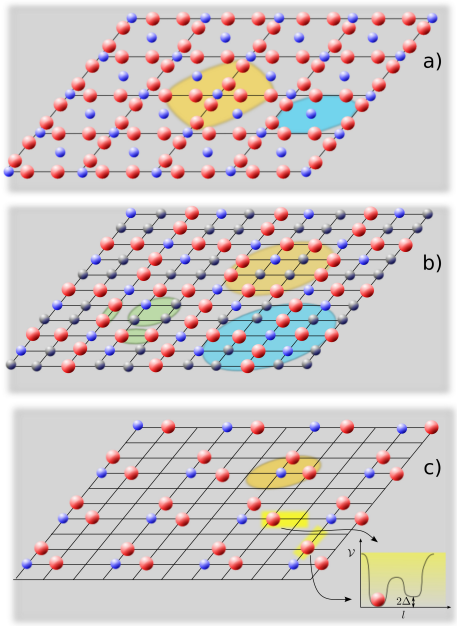

Figure 3. *Lattices of Rydberg atoms* needed for simulating SU(2)-gauge magnets. a) Holographic lattice scheme for the simulation of the pure LGT at weak coupling. Blue spheres represent the "control" two-level atoms, while red spheres are the "ensemble" two-level atoms. Each control atom is surrounded by eight ensemble atoms. The latter are arranged geometrically inside the blockade radius of the control atom. The blockade radii for a plaquette-control atom and the cross-control atom are shaded in cyan and orange, respectively. Single-site addressing is essential for acting selectively on each atom. b) An different lattice scheme has to be used to introduce static charges. It is made from super-sites including four two-level atoms (shaded green circle). One of these is a cross-control atom (blue) while the other three are used to encode static charges (black). Single-site addressing makes it possible to use i) only one of the charge qubits (having matter with spin 1/2) or ii) several charge qubits (representing static charges with possible total spin $1/2, 1, 3/2$). The links of the gauge magnets, which connect these effective sites, have two atoms each (red spheres on shaded green oval). Inside the blockade radius of the cross-control atom, there are now eight atoms encoding the gauge magnet constituents (on the four links entering the site) and three charge qubits at the super-site (the region shaded in orange). Inside the blockade radius of the plaquette-control atom, there are several Rydberg atoms. Using single-site addressing, some of them are not used by the mesoscopic Rydberg gates needed to encode plaquette terms of H in (8). Indeed we selectively act only on the eight atoms of the gauge-magnet links around that plaquette (the blockade region is shaded in cyan). c) At strong coupling, the lattice can be considerably simplified. The plaquette-control atoms are absent (the Hamiltonian has no plaquette term) so that the number of control atoms is halved. We can also half the number of atoms per link, reducing it to one atom per link. Indeed, we replace the atoms encoding the position qubits with a double-well potential at each link; following (8) the relative height of the two potential wells differs by 2Δ. Since spin qubits in the ground state are in $|0\rangle$, corresponding to the left (lower) well of the potential for x (y) links, the right (up) well is empty and the system is at half-filling. In order to implement (5) the blockade radius of the cross-controls can be limited to the first four wells around a site (shaded in cyan).

invariance, $\tilde{\Delta} \sim \Delta/g$.

The adiabatic approximation is justified by choosing T large enough compared to the inverse of the gaps of H and H_G, which are both finite. The time-evolution operator acting on a state is implemented by a sequence of basic eight-qubit controlled rotations. Each of them involves two Rydberg gates and several single-qubit rotations (cf. [28]). The number of terms in this sequence poses an upper bound on the temperature of the system (see Methods).

The same procedure is used to obtain ii), the ground state with two, or more, static charges. Their presence is accounted by placing new atoms on the sites of the lattice and enforcing (10). A possible lattice scheme that accommodates several choices of static charges is presented in Fig. 3 b). There the sites are made by four neighboring potential wells and can host, apart from the control, up to three further atoms. The lattice spacing is chosen such that the desired atoms are inside the blockade radius of the respective controls (shaded in Fig. 3 b)).

Regarding iii), we identify two strategies to detect confinement. At a qualitative level, the string of singlets joining the two charges can be detected by using spin-polarization spectroscopy [40]. At a quantitative level, a direct measurement of the energy can be performed following the same approach used to perform the time evolution and reading out by fluorescence [41] the control qubits.

What we have described so far is experimentally challenging but can be used to probe confinement at $g \to 0$ with all the plaquettes on. This has been conjectured in [36]. Experimentally confinement would manifest through the shape of the energy-excess around the static charges, as an energy concentration along a tube joining the two charges. On the contrary, free charges would lead to spreading of the energy, footprint of a dipolar potential.

In the *strongly-coupled* regime, we can perform a simplified experiment. Energy depends only on the position qubit of each link, with the state $|0\rangle$ ($|1\rangle$) favored (penalized) by Δ. Hence, we perform a partial *analog* encoding by placing the spin qubits in a super-lattice producing a double-well potential $\mathcal{V}$ on each link, see Fig. 3 c). The two wells play the role of the position qubits and have an off-set of 2Δ.

When two static charges are added to the system, we need to introduce two extra atoms above the half filled ground state. The creation of the strings described in the previous section can be mimicked by driving the system with $e^{-i\int_0^T \lambda(t) H_G \mathrm{dt}}$, $\tilde{\Delta} > 2\Delta$, while simultaneously inducing in-well atom oscillations via AC-shaking [42] of the lattice at 45°. Adjusting the intensity of the shaking, we allow for the adiabatic adjustment of the atoms, which then freeze in minimal energy configurations compatible with gauge invariance. The strings can be observed by direct imaging of the atoms positions, e.g., by joining those atoms found at the right (up) end of the x (y) links.

Note that the number of sequential Rydberg gates to be performed in a time step of the state preparation is 36, i.e., small enough to satisfy $\tilde{\Delta} \gg$ thermal excitations ($\sim$ 1/100 Rydberg gate times) in current experiments (assuming a Rydberg gate frequency $\sim 1/\mu$s, and an experimental temperature $\sim 10^{-8}$ °K).

Summarizing, we have proposed a quantum simulator of non-Abelian LGT, based on non-Abelian gauge magnets (for similar proposals see [43, 44]). We have identified the mechanism producing charge confinement in this model. We have characterized its intrinsic non-Abelian nature through the part of the LRE generated by a single string configuration. We have designed experiments that allow to prepare the ground state and mimic the physics of charge confinement. This is only the first step towards the full quantum simulation of full-fledged QCD. Note that a slight modification of the model considered here allows for a relativistic dispersion relation as required by QCD [36]. The physics we described here is dominated by the presence of singlets, that play a fundamental role in high-temperature superconductivity. We foresee that the experiments we propose provide also new insights in this area (see also [45, 46]). An interesting development would be to apply the ideas of [47, 48] to measure in the experiments the intrinsic LRE carried by a single chromo-electric string.

We acknowledge support from TOQATA (FIS2008-00784), FP7-PEOPLE-2010-IIF ENGAGES 273524, ERC QUAGATUA, and EU AQUTE.

METHODS

Quantum gates for Coherent evolution

In the following, we give the explicit form of the driving W and its engineering in terms of Rydberg gates. In particular, we discuss the upper bound on the energy scale of the system required by the validity of the Trotter approximation. As the consequence, such bound translates in upper bound on the temperature of the atomic sample.

Let us start with plaquette term. From the explicit form of the operator $U = \sigma_1 \otimes \sigma^0 \otimes \tau^0 - i\sum_{j=1}^{3} \sigma_2 \otimes \sigma^j \otimes \tau^j$, it follows that the Hamiltonian, for $g \to 0$, is $H = \frac{\Delta}{g} \sum_p H_p$, with

$$H_p = \mathrm{tr}(U \otimes U \otimes U^\dagger \otimes U^\dagger$$

$$= 2\Bigg[\sigma^{1\otimes 4}\otimes\sigma_0{}^{\otimes 4}+\sum_j\Big(\sigma_1{}^{\otimes 2}\otimes\sigma_2{}^{\otimes 2}\otimes\sigma^{0\otimes 2}\otimes\sigma^{j\otimes 2}+5\text{perm.}\Big)$$
$$+\sigma_2{}^{\otimes 4}\otimes\left(\sum_{i,j}\sigma^{i\otimes 2}\otimes\sigma^{j\otimes 2}+\sum_{i\neq j}\sigma^i\otimes\sigma^{j\otimes 2}\otimes\sigma^i-\sum_{i\neq j}(\sigma^i\otimes\sigma^j)^{\otimes 2}\right)$$
$$-\sum_{i,j,k}\epsilon^{ijk}\left(\sigma_1\otimes\sigma_2{}^{\otimes 3}\otimes\sigma^0\otimes\sigma^i\otimes\sigma^j\otimes\sigma^k+\sigma_2\otimes\sigma_1\otimes\sigma_2{}^{\otimes 2}\otimes\sigma^i\otimes\sigma^0\otimes\sigma^j\otimes\sigma^k\right)+$$
$$+\sum_{i,j,k}\epsilon^{ijk}\left(\sigma_2{}^{\otimes 2}\otimes\sigma_1\otimes\sigma_2\otimes\sigma^i\otimes\sigma^j\otimes\sigma^0\otimes\sigma^k+\sigma_2{}^{\otimes 3}\otimes\sigma_1\otimes\sigma^i\otimes\sigma^j\otimes\sigma^k\otimes\sigma^0\right)\Bigg], \quad (12)$$

where σ^0 is the 2x2 identity matrix and ϵ^{ijk} is the Levi-Civita symbol. The indices i,j,k in the sums go from 1 to 3. For simplicity, in the above expression we omit subscripts indicating links and plaquette. For convenience, the operator H_p is written in the form $\mathcal{P}^{\otimes 4}\otimes\mathcal{S}^{\otimes 4}$.

Hence, H_p is a sum of 64 monomial tensor products of σ^μ, $\mu=0,1,2,3$, that are not commuting, although some pairs of them are. Formally, we can write

$$H_p=\sum_{J=1}^{64}Q_p^{(J)},\ Q_p^{(J)}\equiv\bigotimes_{n=1}^{8}\sigma^{\mu_n^{(J)}}. \quad (13)$$

Let us now consider the gauge condition (5). Defining $H_G=-\tilde{\Delta}\sum_s H_s=-\tilde{\Delta}\sum_{s,\vec{\alpha}=\alpha\hat{x},\alpha\hat{y},\alpha\hat{z}}(G_s(\vec{\alpha})+G_s(\vec{\alpha})^\dagger)$, we have an adjoint operator by construction that can serve as part of the Hamiltonian. It follows that also H_s can be written as a sum of monomials of σ_μ. Indeed, we have

$$H_s=\sum_j\left(\left(\frac{1+\cos\alpha}{2}\sigma_0+\frac{1-\cos\alpha}{2}\sigma_3\right)\otimes\sigma^0+i\sin\alpha\frac{\sigma_0-\sigma_3}{2}\otimes\sigma^i\right)^{\otimes 2}\otimes$$
$$\otimes\left(\left(\frac{1+\cos\alpha}{2}\sigma_0-\frac{1-\cos\alpha}{2}\sigma_3\right)\otimes\sigma^0+i\sin\alpha\frac{\sigma_0+\sigma_3}{2}\otimes\sigma^i\right)^{\otimes 2}+H.c.. \quad (14)$$

As the decomposition is a very lengthy expression, we count the total number of monomials. The Hermitian terms are the ones containing even powers of $\sin\alpha$. For a given j, we have $\binom{4}{0}2^4\times(\sin\alpha)^0$ terms, plus $\binom{4}{2}2^4\times(\sin\alpha)^2$ terms, plus $\binom{4}{4}2^4\times(\sin\alpha)^4$ terms. As the $(\sin\alpha)^0$-terms are the same for any $j=1,2,3$, the total number of terms is $(1+3\times 7)2^4=352$. Hence, formally we can write

$$H_s=\sum_{J=1}^{352}Q_s^{(J)},\ Q_s^{(J)}\equiv\bigotimes_{n=1}^{8}\sigma^{\mu_n^{(J)}}. \quad (15)$$

As explained in the main text, the adiabatic preparation requires also an auxiliary gapped Hamiltonian H_a that has the configuration we start with as unique ground state. Such a H_a ensures that the unitary evolution

$$W=e^{-i\int_0^T H(t)\mathrm{d}t}\sim\prod_{t=0}^{t=T}e^{-i\int_t^{t+\delta t}(1-\lambda(t'))H_a\mathrm{d}t'}$$

$$e^{-i\int_t^{t+\delta t}\lambda(t')(H+H_G)\mathrm{d}t'}\equiv\prod_{t=0}^{t=T}W(t), \quad (16)$$

is adiabatic for $\lambda(t)\ll 1$, *i.*e. $t\ll T$. A suitable choice for the initial state is $\prod_{l_h}(|+\rangle\otimes|1\rangle)\prod_{l_v}(|+\rangle\otimes|0\rangle)$, where l_h and l_v are the horizontal and the vertical links of the lattice, respectively, and $|+\rangle\equiv\frac{1}{\sqrt{2}}(|0\rangle+|1\rangle)$, so that it has non-zero overlap with $|\Omega_0\rangle$ of (11). A consequent suitable choice for H_a is

$$H_a=-\tilde{\Delta}\left(\sum_{l_h}(\sigma_1\otimes\sigma^0-\sigma_0\otimes\sigma^1)\sum_{l_h}(\sigma_1\otimes\sigma^0-\sigma_0\otimes\sigma^1)\right),$$

which is very easy to implement in terms of single-qubit rotations.

It is worth to notice that alternative plaquette terms (to the one we consider here) and the electric term $\Delta\sum_s\Gamma^5=\sum_l\sigma_3\otimes\sigma^0$ can be also easily decomposed in monomials of σ_μ and implemented as explained below.

Now we are able to compute the driving operator W in terms of the Q's. Indeed, we have

$$e^{i\int_t^{t+\delta t}(1-\lambda(t'))H_a \mathrm{d}t'} W(t) = e^{-i\int_t^{t+\delta t}\lambda(t')(\tilde{\Delta}\sum_s H_s + \frac{\Delta}{g}\sum_p H_p)\mathrm{d}t'} = e^{-i\int_t^{t+\delta t}\lambda(t')\tilde{\Delta}\sum_{s,J} Q_s^{(J)}\mathrm{d}t'} e^{-i\int_t^{t+\delta t}\lambda(t)\frac{\Delta}{g}\sum_{p,J} Q_p^{(J)}\mathrm{d}t'}, \quad (17)$$

since the two Hamiltonians commutes by construction, due to (7). The driving is efficient as, for $\Delta, \tilde{\Delta} \neq 0$, H and H_G are both gapped, with gaps proportional to Δ and $\tilde{\Delta}$, respectively.

Note that the scale $\tilde{\Delta}$ has to chosen appropriately. In absence of charges, as $[H_G, H] = 0$ and $|\Omega_0\rangle$ is the simultaneous minimum of both H and H_G, it is sufficient to take $\tilde{\Delta} \sim \Delta/g$. However, when charges are present, the ground state is an eigenvector of H, but not with minimal eigenvalue, if we do not limit the Hilbert space to the gauge-invariant subspace. We ensure that this is the case by requiring that the ground state minimizes H_G, *i*.e. requiring $\tilde{\Delta}$ sufficiently greater than Δ/g, precisely $\tilde{\Delta} > ||H||$.

As explained in [33] and [28], any term of the form $e^{i\alpha Q^{(J)}}$ can be implemented, up to single-qubit rotations, by applying the mesoscopic Rydberg gate twice. Hence, we can expand in Trotter approximation any of the two exponentials in (17) in product of exp of the Q's and realize the evolution as a sequence of gates. For instance,

$$e^{-i\lambda(t)\frac{\Delta}{g}\sum_{p,J} Q_p^{(J)}} = \left(e^{-i\frac{\lambda(t)}{N}\frac{\Delta}{g}\sum_{p,J} Q_p^{(J)}}\right)^N \sim \prod_J \left(e^{-i\frac{\lambda(t)}{N}\frac{\Delta}{g}\sum_p Q_p^{(J)}}\right)^N, \text{ for } \frac{\lambda(t)}{N}\frac{\Delta}{g} \ll 1. \quad (18)$$

The crucial point to be noticed is that N cannot be arbitrary large. In order to perform a time-step of evolution, our Rydberg apparatus physically needs a time $T_{step} = 2\#$ of Q's $\times t_R$, where t_R is the delay of a single Rydberg gate. It follows that

$$\frac{\Delta}{g} \ll \frac{1}{T_{step}}, \quad (19)$$

which for the plaquette term above, without further optimization, is of order $\frac{1}{T_{step}} \sim 10^2$ KHz, while for the gauge term is about five time smaller. This means that ground state and dynamics in a generic regime of (8) requires a considerably cold atomic sample, about one order of magnitude colder than in present experiments. However, we do not discard that the above implementation can be improved and made less demanding applying gate optimization.

Strong coupling experiment

The situation improves considerably in the simplified scheme we propose in the strong coupling limit. Indeed, as the dynamics and, partially, the structure of Hilbert space are encoded directly in the lattice, we have to perform only the coherent evolution of an exponentially simpler gauge condition: the cross operator acts on only four qubits as in the Abelian case [28], instead of eight. The new H_s is

$$H_s = \sum_{j=1}^{3}(e^{i\sigma^j})^{\otimes 4} = 2(\cos\alpha)^4\sigma^{0\otimes 4} + -2(\cos\alpha\sin\alpha)^2(\sigma^{j\otimes 2}\otimes\sigma^{0\otimes 2} + 5\text{perm.}) + (\sin\alpha)^4\sigma^{j\otimes 4},$$

and the only non-trivial terms that we have to engineer with Rydberg gates are 18, *i*.e. $T_{step} = 36t_R$. As briefly mentioned in the main text, such T_{step} is sufficiently smaller than the typical time-scale associated to (the inverse of) thermal fluctuations in current state-of-art experiments, $T \lesssim 10^{-8}\ ^\circ K$.

We conclude with few comments on AC-shaking procedure. As explained in the main text, we allow the system to reach the minimal energy configuration during the adiabatic evolution by inducing an hopping between the wells forming the links. In this way, the value of the position qubit, *i*.e. the position of the two-levels atom in each well, can change to the less energetic one while satisfying the new gauge condition in presence of charges. The gauge condition determines the configuration of the gauge qubits, forming singlets between pairs of them. An AC-periodic forcing of the lattice can provide this hopping in a selective way. Indeed, the AC-induced hopping is obtained only if the frequency of the forcing ω is commensurable with 2Δ, the relative energy off-set between the two wells, *i*.e. $\Delta = \frac{\nu}{2}\hbar\omega$, ν integer [49]. This is sufficient to avoid the generation of unwanted tunneling terms as, for instance, of the control atom to the link wells and vice-versa. Furthermore, other unwanted hopping terms between different links are strongly suppressed by the exponential decay of Wannier functions. In order to induce the same rate of in-well oscillations for horizontal and vertical links, the periodic forcing $\vec{F}$ is chosen to be parallel to the plane at a 45° angle, $\vec{F} \parallel (1,1,0)$.

* luca.tagliacozzo@icfo.es
† alessio.celi@icfo.es

[1] L. O'Raifeartaigh and N. Straumann, Reviews of Modern Physics **72**, 1 (2000).
[2] M. K. Gaillard, P. D. Grannis, and F. J. Sciulli, Reviews of Modern Physics **71**, S96 (1999).
[3] A. V. Smilga, *Lectures on Quantum Chromodynamics* (World Scientific, 2001).
[4] L. Balents, Nature **464**, 199 (2010).
[5] P. A. Lee, N. Nagaosa, and X.-G. Wen, Reviews of Modern Physics **78**, 17 (2006).
[6] A. Mann, Nature News **475**, 280 (2011).
[7] A. Kitaev, Annals of Physics **303**, 2 (2003).

[8] S. Trebst, P. Werner, M. Troyer, K. Shtengel, and C. Nayak, Physical Review Letters **98**, 070602 (2007).

[9] I. S. Tupitsyn, A. Kitaev, N. V. Prokof'ev, and P. C. E. Stamp, Physical Review B **82**, 085114 (2010).

[10] L. Tagliacozzo and G. Vidal, Physical Review B **83**, 115127 (2011).

[11] S. Dusuel, M. Kamfor, R. Orús, K. P. Schmidt, and J. Vidal, Physical Review Letters **106**, 107203 (2011).

[12] K. G. Wilson, Physical Review D **10**, 2445 (1974).

[13] A. Bazavov, D. Toussaint, C. Bernard, J. Laiho, C. DeTar, L. Levkova, M. B. Oktay, S. Gottlieb, U. M. Heller, J. E. Hetrick, P. B. Mackenzie, R. Sugar, and R. S. Van de Water, Reviews of Modern Physics **82**, 1349 (2010).

[14] A. M. Polyakov, Physics Letters B **59**, 82 (1975).

[15] P. C. Kim, E. R. Lee, I. T. Lee, M. L. Perl, V. Halyo, and D. Loomba, Physical Review Letters **99**, 161804 (2007).

[16] H. Satz, Physics Reports **403–404**, 33 (2004).

[17] S. Gupta, X. Luo, B. Mohanty, H. G. Ritter, and N. Xu, Science **332**, 1525 (2011).

[18] A. Collaboration, Physical Review Letters **109**, 072301 (2012).

[19] S. Collaboration, Physical Review Letters **108**, 202301 (2012).

[20] P. W. Anderson, Science **235**, 1196 (1987).

[21] M. Lewenstein, A. Sanpera, and V. Ahufinger, *Ultracold Atoms in Optical Lattices: Simulating quantum many-body systems* (Oxford University Press, USA, 2012).

[22] P. Hauke, F. M. Cucchietti, L. Tagliacozzo, I. Deutsch, and M. Lewenstein, Reports on Progress in Physics **75**, 082401 (2012).

[23] I. Bloch, J. Dalibard, and S. Nascimbène, Nature Physics **8**, 267 (2012).

[24] R. Blatt and C. F. Roos, Nature Physics **8**, 277 (2012).

[25] A. Aspuru-Guzik and P. Walther, Nature Physics **8**, 285 (2012).

[26] A. A. Houck, H. E. Türeci, and J. Koch, Nature Physics **8**, 292 (2012).

[27] E. Zohar, J. I. Cirac, and B. Reznik, Physical Review Letters **109**, 125302 (2012).

[28] L. Tagliacozzo, A. Celi, A. Zamora, and M. Lewenstein, arXiv:1205.0496 (2012).

[29] D. Banerjee, M. Dalmonte, M. Müller, E. Rico, P. Stebler, U.-J. Wiese, and P. Zoller, arXiv:1205.6366 (2012).

[30] E. Zohar, J. I. Cirac, and B. Reznik, arXiv:1208.4299 (2012).

[31] E. Zohar and B. Reznik, arXiv:1208.1012 (2012).

[32] M. Müller, I. Lesanovsky, H. Weimer, H. P. Büchler, and P. Zoller, Physical Review Letters **102**, 170502 (2009).

[33] H. Weimer, M. Müller, I. Lesanovsky, P. Zoller, and H. P. Büchler, Nat. Phys. **6**, 382 (2010).

[34] P. Schauß, M. Cheneau, M. Endres, T. Fukuhara, S. Hild, A. Omran, T. Pohl, C. Gross, S. Kuhr, and I. Bloch, Nature **491**, 87 (2012).

[35] D. Horn, Physics Letters B **100**, 149 (1981).

[36] P. Orland and D. Rohrlich, Nuclear Physics B **338**, 647 (1990).

[37] S. Chandrasekharan and U. Wiese, Nucl.Phys. **B492**, 455 (1997), hep-lat/9609042.

[38] M. A. Levin and X.-G. Wen, Physical Review B **71**, 045110 (2005).

[39] W. S. Bakr, J. I. Gillen, A. Peng, S. Folling, and M. Greiner, Nature **462**, 74 (2009).

[40] K. Eckert, O. Romero-Isart, M. Rodriguez, M. Lewenstein, E. S. Polzik, and A. Sanpera, Nat Phys **4**, 50 (2008).

[41] J. F. Sherson, C. Weitenberg, M. Endres, M. Cheneau, I. Bloch, and S. Kuhr, Nature **467**, 68 (2010).

[42] P. Hauke, O. Tieleman, A. Celi, C. Ölschläger, J. Simonet, J. Struck, M. Weinberg, P. Windpassinger, K. Sengstock, M. Lewenstein, and A. Eckardt, Physical Review Letters **109**, 145301 (2012).

[43] D. Banerjee, M. Dalmonte, M. Müller, E. Rico, P. Stebler, U.-J. Wiese, and P. Zoller, private communication (2012).

[44] E. Zohar, J. I. Cirac, and B. Reznik, private communication (2012).

[45] S. Trebst, U. Schollwöck, M. Troyer, and P. Zoller, Physical Review Letters **96**, 250402 (2006).

[46] S. Nascimbène, Y.-A. Chen, M. Atala, M. Aidelsburger, S. Trotzky, B. Paredes, and I. Bloch, Physical Review Letters **108**, 205301 (2012).

[47] D. A. Abanin and E. Demler, Physical Review Letters **109**, 020504 (2012).

[48] J. Cardy, Physical Review Letters **106**, 150404 (2011).

[49] A. Eckardt and M. Holthaus, Europhysics Letters (EPL) **80**, 50004 (2007).